Time-dependent correlations in a supercooled liquid from nonlinear fluctuating hydrodynamics

Bhaskar Sen Gupta,[1] Shankar P. Das,[1] and Jean-Louis Barrat[2]
[1]*School of Physical Sciences, Jawaharlal Nehru University, New Delhi - 110067, India*
[2]*Université de Lyon, Université de Lyon I, Laboratoire de Physique de la Matière Condensée et des Nanostructures, CNRS, UMR 5586, 43 Boulevard du 11 Novembre 1918, F-69622 Villeurbanne Cedex, France*
(Received 6 January 2011; published 26 April 2011)

We solve numerically the equations of nonlinear fluctuating hydrodynamics (NFH). A coarse graining of the density field is applied at each time step to avoid instabilities which otherwise plague the algorithm at long times. The equilibrium correlation of the density fluctuations at different times obtained directly from the solutions of the NFH equations are shown here to be in quantitative agreement with corresponding molecular dynamics simulation data. Low-order perturbative treatment of the these NFH equations obtains the mode coupling model. The latter has been widely studied for understanding the slow dynamics characteristic of the supercooled state. A crucial aspect of this theory is a rounded version of a possible ergodic-nonergodic transition in the supercooled liquid at a temperature T_c between melting point T_m and the glass transition temperature T_g. In the present work we demonstrate numerically the role of strongly coupled density fluctuations in giving rise to slow dynamics and how the $1/\rho$ nonlinearity in the NFH equations of motion is essential in restoring the ergodic behavior in the liquid. The relaxation data indicate that at moderate supercooling near T_c, the time temperature superposition holds. The relaxation gets increasingly stretched with increased supercooling. The relaxation time τ shows an initial power-law divergence approaching a transition temperature T_c generally identified as the mode coupling temperature. From the direct solutions we obtain a value for T_c much lower than that typically estimated from solution of low-order integral equations of mode coupling theory. This is in agreement with the trend seen in computer simulations.

DOI: 10.1103/PhysRevE.83.041506 PACS number(s): 64.70.Q−, 61.20.Lc, 61.20.Ja

I. INTRODUCTION

The conserved densities of mass, momentum, and energy constitute the simplest set of slow modes which is characteristic of an isotropic liquid. The dynamic behavior of these liquids is often determined in terms of the correlation of fluctuations in these slow modes at different times. The microscopic balance equations satisfied by these slow modes correspond to the respective conservation laws for the relevant physical property, i.e., mass, momentum, and energy. These equations also form the basis of the nonlinear fluctuating hydrodynamics (NFH) model for the dynamics of these slow modes in terms of nonlinear differential equations having regular and stochastic parts. The different terms in these equations thus represent widely different time scales of variation signifying the complex nature of the time evolution of the dense liquid. The regular parts in the NFH equations involve nonlinear coupling of slow modes, while the random parts represent noise which can be linear [1–3] or multiplicative [2,4].

The most widely studied theoretical model for the slow dynamics characteristic of a supercooled liquid approaching vitrification is termed as the self-consistent mode coupling theory (MCT) [5–7], and can be obtained from the NFH equations. The basic idea implemented in the MCT model is that in a strongly interacting dense liquid, the coupling of density fluctuations is dominant and gives rise to a nonlinear feedback mechanism [5] which produces extremely slow dynamics. In its simplest version the MCT predicts that above a critical density, the long time limit of the time correlation $\mathcal{C}(t)$ of density fluctuations is nonzero. This signifies an ergodic-nonergodic transition (ENE) in the liquid at a temperature T_c. This dynamic transition is considered to be a precursor to the liquid-glass transition which occurs in the deeply supercooled liquid at a temperature $T_g < T_c$. The relaxation time of the liquid crosses the typical laboratory time scales at T_g. The dynamics of the supercooled liquid near T_c involves several different regimes of relaxation and has been widely used in fitting experimental data on different liquids. However, the simple MCT approach is known to exaggerate the tendency to produce a slow dynamics, predicting a complete freezing at a rather low density or high temperature. In this regard it is useful to note that the perturbation expansion for the renormalized transport coefficients used in the MCT, though systematic, is in terms of a dimensionless parameter which is not small. It has also been shown [1,8] that the $1/\rho$ nonlinearities in the NFH equations remove the sharp ENE transition predicted in the simplified theory. Thus, in seeking agreement to experiments, the coupling constants appearing in the low-order perturbative model of MCT have often been used as free parameters in obtaining a satisfactory fit with experimental data. However, a first-principles treatment of the dynamics avoiding the low-order perturbation theory and adjustable fit parameters has not been attempted. In the present work we study the consequences of the nonlinear coupling of the density fluctuations in a nonperturbative manner using numerical methods. We report here the study of the slow dynamics of a dense monatomic Lennard-Jones liquid by numerically solving the stochastic equations of NFH. Our nonperturbative calculation shows good agreement with the direct computer simulation results of the same system in equilibrium and demonstrates the roles of the various nonlinearities on the asymptotic dynamics.

II. EQUATIONS OF NFH

We present below a brief description of the equations of fluctuating hydrodynamics which we solve numerically to

compute the correlation functions. For an isotropic liquid we consider the model equations for the mass density ρ and momentum density $\mathbf{g}$ [1] in the simplest form as follows:

$$\frac{\partial \rho}{\partial t} + \nabla \cdot \mathbf{g} = 0, \tag{1}$$

$$\frac{\partial g_i}{\partial t} + \nabla_j \left[\frac{g_i g_j}{\rho} \right] + \rho \nabla_i \frac{\delta F_U}{\delta \rho} + L_{ij} \frac{g_j}{\rho} = \theta_i. \tag{2}$$

The correlations of the Gaussian noise θ_i are related to the bare damping matrix L_{ij} [9],

$$\langle \theta_i(x,t)\theta_j(x't')\rangle = 2k_B T L_{ij}\delta(t-t')\delta(x-x'). \tag{3}$$

For an isotropic liquid, the bare transport coefficients are obtained as

$$L_{ij} = (\zeta_0 + \eta_0/3)\delta_{ij}\nabla^2 + \eta_0 \nabla_i \nabla_j, \tag{4}$$

where ζ_0 and η_0, respectively, denote the bare bulk and shear viscosities. The stationary solution of the Fokker-Planck equation corresponding to the generalized Langevin equation (2) is obtained as $\exp\{-\beta F[\rho,g]\}$ with $\beta = 1/k_B T$ is the Boltzmann factor. The coarse-grained free energy functional is obtained as

$$F[\rho,g] = F_K[\rho,g] + F_U. \tag{5}$$

The kinetic part is dependent on the momentum density

$$F_K = \int d\mathbf{x}\, g^2/(2\rho), \tag{6}$$

and the so-called potential part is given by

$$F_U = F_{\rm id} + F_{\rm int}, \tag{7}$$

where $F_{\rm id}$ represents the purely entropic contributions related to the noninteracting system. This part termed as the ideal gas contribution is obtained in the form:

$$\beta F_{\rm id} = \int d\mathbf{r}\rho(\mathbf{r}) \left[\ln\left(\frac{\rho(\mathbf{r})}{\rho_0} \right) - 1 \right]. \tag{8}$$

The interaction part $F_{\rm int}$ up to quadratic order in density fluctuations [10] is obtained as

$$\beta F_{\rm int} = -\frac{1}{2m^2} \int d\mathbf{r}\, d\mathbf{r}' c(\mathbf{r}-\mathbf{r}')\delta\rho(\mathbf{r})\delta\rho(\mathbf{r}'), \tag{9}$$

where $c(r)$ is the two point Ornstein-Zernike direct correlation function [9] and m is the mass of the particles.

For the glassy dynamics we focus on the coupling of slowly decaying density fluctuations present in the pressure functional, represented by the third term on the left-hand side of Eq. (2). With the choice of F_U as presented above in Eqs. (7)–(9), the nonlinear contribution in this term reduces to

$$\rho \nabla_i \frac{\delta F_U}{\delta \rho} = \rho \nabla_i f(r,t), \tag{10}$$

with the function $f(r,t)$ being presented in the form of a convolution

$$f(\mathbf{r},t) = m^{-1} \int d\mathbf{r}\, c(\mathbf{r}-\mathbf{r}')\delta\rho(\mathbf{r}',t). \tag{11}$$

If we replace ρ by ρ_0 in the right-hand side of Eq. (10) then we have a dynamics linearized in density fluctuations.

III. NUMERICAL SOLUTION OF NFH EQUATIONS

We now present the steps followed in solving the above-described NFH equations numerically on a cubic grid with mesh size h in three dimensions. We consider here a classical system of N particles, each of mass m interacting via the Lennard-Jones potential

$$u(r) = 4\epsilon \left[\left(\frac{\sigma}{r} \right)^{12} - \left(\frac{\sigma}{r} \right)^{6} \right]. \tag{12}$$

The present problem therefore involves two characteristic length scales: the scale σ of the interacting potential, and length h of the cubic lattice grid on which ρ and $\mathbf{g}$ are computed. The ratio σ/h is chosen to be noninteger $=4.6$ to reduce the likelihood of crystallization in the system. In the results presented here, time is scaled with the Lennard-Jones (LJ) unit of $\tau_0 = (m\sigma^2/\epsilon)^{\frac{1}{2}}$, and length with h. The thermodynamic state of the fluid is described in terms of the reduced density $n^* = n_0\sigma^3$ and the reduced $T^* = (k_B T)/\epsilon$. For numerical solution the conserved densities are scaled to dimensionless forms:

$$n(\mathbf{r}) = [h^3 m^{-1}]\rho(\mathbf{r}), \quad \mathbf{j}(\mathbf{r}) = \left[h^3 (m\epsilon)^{-\frac{1}{2}}\right]\mathbf{g}(\mathbf{r}). \tag{13}$$

A microscopic frequency for the liquid state corresponding to fluctuations at wave number q is obtained as $\Omega_q = q/[\beta m S(q)]$. The inverse Ω_q represents a microscopic time scale for the system. The speed of sound c_0 in the hydrodynamic limit is given by $c_0^2 = k_B T/[m S(0)]$.

The numerical solution scheme used here starts with an initial distribution of the fluctuating variables $n(\mathbf{r})$ and $\mathbf{j}(\mathbf{r})$ over a set of points 20^3 on a cubic lattice. The equation of motion for the density variable $\rho(x,t)$, i.e., the continuity equation, is linear. Let us consider the various nonlinear terms present in the equation of motion for the momentum density. First, the nonlocal integral $f(r,t)$ defined in Eq. (11) appears in the reversible part of the equation of motion and is evaluated as a sum of contributions from the successive shells,

$$f(r,t) = h^3 \sum_i c(R_i) \sum_\alpha \delta n\left(R_i^\alpha, t\right), \tag{14}$$

where R_i^α for $\alpha = 1, \ldots, m_i$ denotes radii vectors of the m_i lattice points in the ith spherical shell of radius R_i. Second, the $1/\rho$ nonlinearity in the dissipative term of the momentum equation is computed by replacing the density field in the denominator with the $\rho(\mathbf{x})$ averaged over a length scale close to σ around the corresponding point $\mathbf{r}$. Finally, we ignore the convective nonlinearity in the present calculation and focus on the role of the pressure nonlinearity in producing the slow dynamics.

A major hurdle encountered in the numerical scheme used here arises from an instability which occurs from the numerical artifact in the solution scheme by which $n(\mathbf{x},t)$ becomes negative at certain grid points. To avoid this situation, we adopt a coarse-graining scheme in which the density $n(\mathbf{x},t)$ on the grid is redefined at each step of the numerical integration. In devising the steps for the coarse graining, we make use of the following physical interpretation of the definition of $\rho(\mathbf{x},t)$ of the density field: the integral $\int_{\Delta V} d\mathbf{x}\, \rho(\mathbf{x},t)$ over an elementary volume ΔV of the system represents the total mass in this volume. To maintain this at each time step of

the numerical integration, the positivity of the field $n(\mathbf{x})$ over the whole grid is checked. If the density turns negative at a point after numerical integration, we reduce $n(\mathbf{x})$ at some or all of the neighboring sites by taking equal contributions from each and add the sum total to the original site. It is also ensured that the density at none of the neighboring sites becomes negative as a result of this redistribution. The sum of the densities at the original and the contributing sites remains unaltered and hence global conservation is maintained at all times. If the above redistribution involving contributions only from the nearest-neighbor sites is insufficient to make $n(\mathbf{x})$ positive everywhere, we include the next-nearest neighbors in the redistribution and so on. In reality, however, it turns out from the execution of the program that we hardly need to include beyond the second shell of neighbors surrounding the original site. With the density instability being corrected with this coarse-graining procedure, the numerical algorithm can be run up to much longer times than in the earlier works [11]. The arbitrary regularization of the strength of the noise [11] is avoided, and the fluctuation dissipation relation is respected in the proper form given in Eq. (3).

Starting from a uniform configuration of density and momentum density on the grid of points, we solve the equations of motion progressively in time and the results for the density fluctuations are saved in selected time bins. The whole array consisting of the density fluctuations $n(\mathbf{x},t)$ at different lattice points $\mathbf{x}$ are then transformed using fast Fourier transform subroutines and stored as $\rho(\mathbf{k},t)$ in selected time bins. These data repeated over different sets of initial conditions are averaged to obtain the correlation functions. From these data the correlation of density fluctuations at two different times is obtained. Equilibrium is inferred for the system when time translational invariance of the correlation function is obtained, i.e., $C(t+t_w,t_w)$ is a function of t only.

IV. EQUILIBRIUM CORRELATION FUNCTIONS

We adopt the above-described method of computing the time correlation functions for the equilibrium system. As a check we compute the equal time correlation function from the solution of the FNH equations. First, we obtain from the density field $\rho(\mathbf{x}_i) \equiv \rho_i$ at the point $\mathbf{x}$ on the grid, the two point pair correlation function $g(r)$ as follows. The latter is defined in terms of the density fields $\{\rho_i\}$ at the different points (denoted by i) on the grid as

$$g(r) = \left\langle \frac{\Sigma_{i>j}\rho_i\rho_j f_{ij}}{\rho_0^2 \Sigma_{i>j} f_{ij}} \right\rangle, \tag{15}$$

where ρ_0 is the average density. The weight function $f_{ij} = 1$ if the separation between mesh points i and j lies between r and $r+\Delta r$ (Δr is a suitably chosen bin size), and $f_{ij} = 0$ otherwise. The angular brackets refer to an average over the noise. We compute this correlation function directly from the density fields computed on the lattice at times when the time translational invariance has been attained indicating a thermally equilibrated state. The equilibrium $g(r)$ vs r plot corresponding to $T^* = 2.0$ and $n_0^* = 0.97$ is displayed in Fig. 1. As it was already pointed out, replacing the ρ in the right-hand side of Eq. (10) with ρ_0, the dynamics gives rise to a linear dynamics and the corresponding numerical solution is trivially obtained with almost no coarse graining. The $g(r)$ obtained with the linear equations of motion is also displayed in the inset of Fig. 1. The coarse graining has some though not drastic influence on the solution as we can see from the difference of the two results.

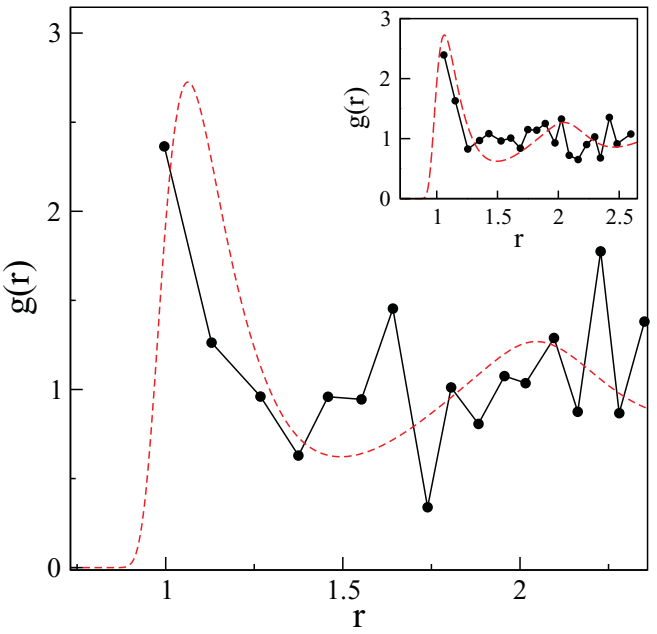

FIG. 1. (Color online) Pair correlation function $g(r)$ vs r (in units of σ) at $T^* = 2$ and $n_0^* = 0.97$ for nonlinear dynamics (line-point) and as computed from input $c(r)$ (dashed line). The corresponding result for the linear case is shown in the inset.

The size of the grid h ($\approx 0.23\sigma$ here) also limits the numerical computation. The solution of the NFH equations involves first and second spatial derivatives of the hydrodynamic fields ρ and $\mathbf{g}$. The accuracy of these numerically calculated derivatives depends on the grid size. And we need to make an optimum choice for limitation with computation time. The effect of this spatial grid size shows up in the static quantities, which show a considerable amount of scatter.

During the process of equilibration, as the system evolves, the corresponding equal time correlation $g(r)$ is obtained at each stage. In Fig. 2 we display for two distances $r = \sigma$ and 2.0σ how the $g(r)$ reaches the respective time-independent value. The corresponding results obtained from the solutions of the the linear equations are also shown in the inset of Fig. 2 for comparison. In this case the equilibration occurs over shorter time scales, since the relaxation time is also shorter.

Next, we use the solutions for the density field $\rho(\mathbf{x},t)$ on the cubic grid to obtain the dynamics of the correlation functions involving two different times. The normalized time correlation of the density fluctuations is defined as

$$C(q,t+t_w,t_w) = \frac{\langle \delta\rho(q,t+t_w)\delta\rho(-q,t_w)\rangle}{\langle \delta\rho(q,t_w)\delta\rho(-q,t_w)\rangle}. \tag{16}$$

where q is the wave vector corresponding to the scale of the fluctuations. We focus here primarily on the density correlation functions at the wave number $q = q_m$. The decay of $C(q_m,t)$ is compared with the results from corresponding molecular

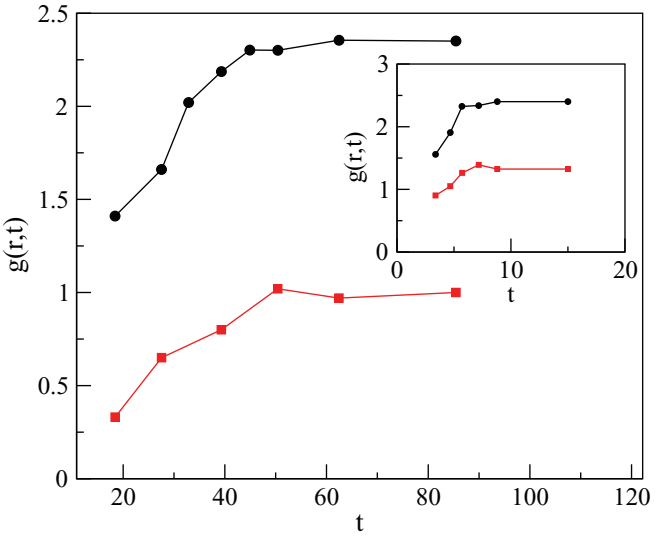

FIG. 2. (Color online) Evolution of the pair correlation function $g(r,t)$ vs t/τ_0 for $r = 1.0$ (circles) and 2.0 (squares) (in units of σ) at $T^* = 2$ and $n_0^* = 0.97$ for nonlinear dynamics. The corresponding result for the linear case is shown in the inset.

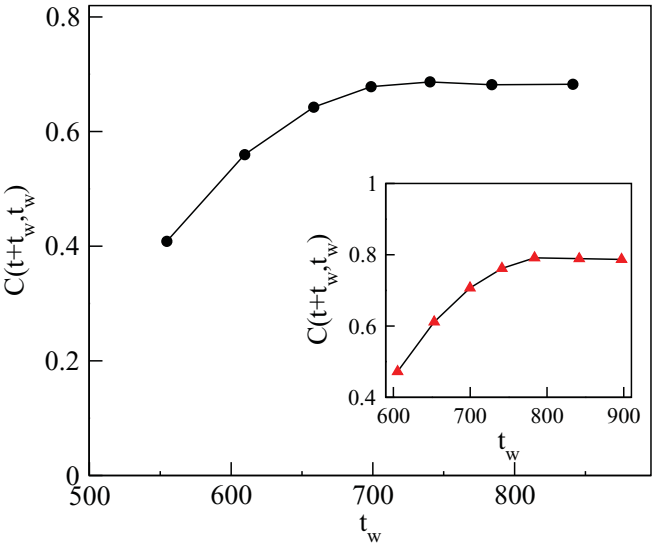

FIG. 3. (Color online) Variation of $C(t+t_w,t_w)$ as a function of t_w/τ_0 at a fixed time $t/\tau_0 = 40$ at $T^* = 0.6$ for density $n_0^* = 1.10$. The corresponding result for density $n_0^* = 1.24$ is shown in the inset.

dynamics (MD) simulation. In comparison to the present approach, MD simulation is a direct reproduction of the microscopic dynamics, and the coordinates of the different constituent particles of the fluid are obtained by solving the equations of motion at the microscopic level. The dynamic correlation function is directly obtained from the microscopic coordinates of the particles and averaged over different initial configurations in this case.

The one-component Lennard-Jones system is often difficult to simulate at supercooled densities avoiding crystallization of the liquid into an ordered state. Ullo and Yip simulated a Lennard-Jones system with only the repulsive part and computed [12] the corresponding time correlation functions using the microscopic coordinates of the particles. The interaction potential between the particles chosen by Ullo and Yip have only the purely repulsive part of the Lennard-Jones interaction, i.e., the so-called cut Lennard-Jones potential [12] defined as follows:

$$u(r) = 4\epsilon\left[\left(\frac{\sigma}{r}\right)^{12} - \left(\frac{\sigma}{r}\right)^{6}\right] + \epsilon \quad \text{for} \quad r \leqslant \sigma_0, \quad (17)$$

$$= 0 \quad \text{for} \quad r > \sigma_0, \quad (18)$$

where $\sigma_0 = 2^{\frac{1}{6}}\sigma_0$. For comparing solutions of the FNH equations with Ullo and Yip's simulation data, we use the input $c(r)$ in the FNH equations to be the same for the above cut Lennard-Jones potential. The bare transport coefficients which determine the noise correlations are chosen such that the short time dynamics agrees with computer simulation results. $\mathcal{C}(t)$ obtained by solving the stochastic equations linearized in the fluctuations decays very fast. We first start with a uniform initial density configuration and let the $\rho(\mathbf{x},t)$ fields driven by the Gaussian noise evolve with time. Generally an evolution up to a time scale of the corresponding α-relaxation time is required to reach the stage in which $C(t+t_w,t_w)$ is a function of time t only. For large t_w as the system equilibrates, time translational invariance holds, making $C(t+t_w,t_w) \equiv \mathcal{C}(t)$. We display convergence to this behavior in Fig. 3 for the two densities $n\sigma^3 = 1.10$ and 1.24. Beyond a time of 700 and 800 (in Lennard-Jones units) for $n\sigma^3 = 1.10$ and 1.24, respectively, we assume the time translational invariance and obtain the corresponding time correlation functions.

In Figs. 4 and 5, correlation functions for the equilibrated systems at $T^* = 0.6$ for two densities $n_0^* = 1.10$ and $n_0^* = 1.24$, respectively, are shown. Considerable slowing down of the decay of $\mathcal{C}(t)$ occurs on solving the full NFH equations. From our comparison the agreement of the numerical solution of the fluctuating hydrodynamic equations with the simulation results seems to be better at $n_0^* = 1.24$ than at 1.10. At higher densities the mean-free path of the fluid particles gets smaller and approaches the atomic length scale. As a result, the validity of generalized hydrodynamic equations at short length scales (corresponding to wave vector $q \sim q_m$) improves with increasing density. This trend is clearly seen in our results displayed in Figs. 4 and 5 for $\mathcal{C}(t)$. In the present calculation we notice that the density correlation functions decay over time and only the relaxation time grows. The corresponding result obtained from the one-loop MCT equations will have the density correlations completely frozen at this density [13].

The numerical solutions of the equations of the NFH which provide nonperturbative results are in much better agreement with simulation data than the usual low-order perturbation theory results for such systems. This agreement is without any adjustable parameter in the theory and demonstrates that the solution of the basic equations of the nonlinear fluctuating hydrodynamics (which is the starting point of MCT) provides the correct dynamics for the dense liquid. While making that observation, it should be noted that the bare transport coefficients have been adjusted here to get agreement with the short time dynamics. However, this does not affect the long time decay of the correlation functions in any significant manner.

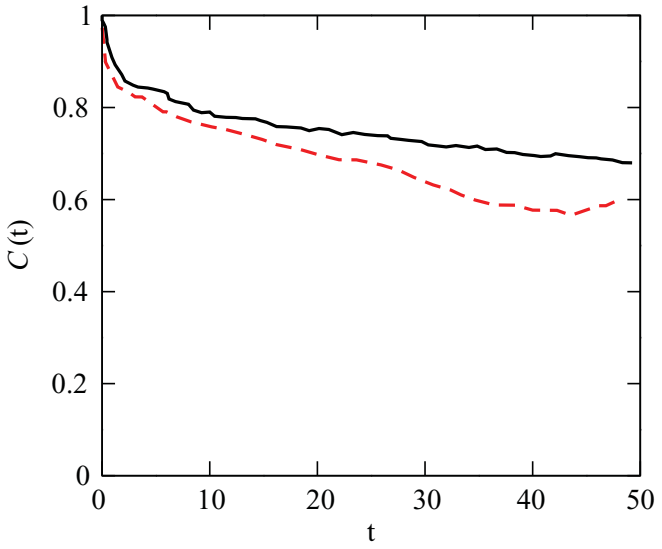

FIG. 4. (Color online) $\mathcal{C}(t)$ vs t/τ_0 graph at $T^* = 0.6$ for density $n_0^* = 1.10$ (solid curve), and the corresponding MD simulation data [12] (dashed curve).

The nonperturbative treatment of the FNH equations presented here and the relations to the low-order MCT results are further understood by analyzing the roles of the specific nonlinearities in the equations of motion. For this we focus on the $1/\rho$ nonlinearity in the dissipative term in Eq. (2). The ENE transition of the simple MCT is driven by the nonlinear couplings of density fluctuations in the pressure term (third term on the left-hand side) of the generalized Navier-Stokes equation. On the other hand the $1/\rho$ nonlinearity crucial for the absence of the ENE transition is in the dissipative term of the same equation, i.e., fourth term on the left-hand side of Eq. (2). We therefore consider two cases here to test the role of the relevant nonlinearities from a nonperturbative approach. In case A the $1/\rho$ nonlinearity in Eq. (2) is replaced with $1/\rho_0$ while keeping the density nonlinearity in

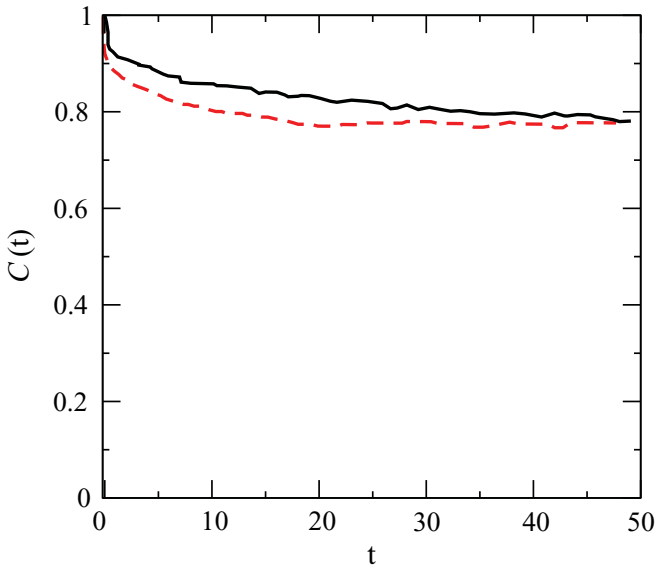

FIG. 5. (Color online) Same as Fig. 4, but for density $n_0^* = 1.24$.

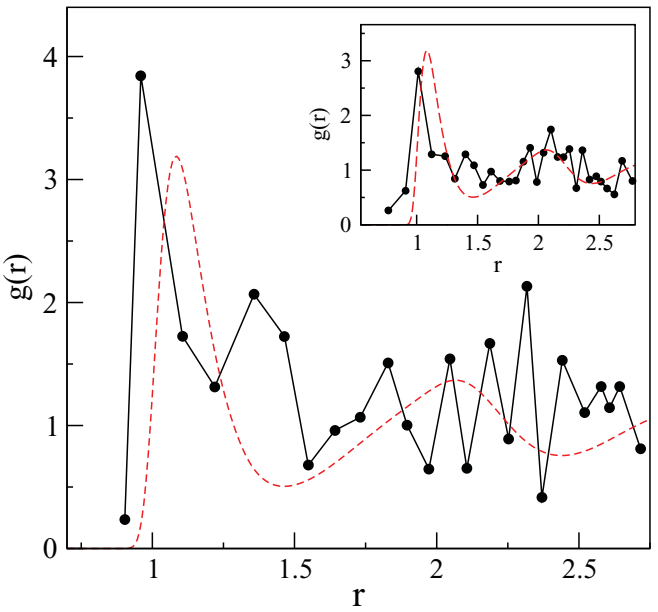

FIG. 6. (Color online) Pair correlation function $g(r)$ vs r (in units of σ) at $T^* = 0.6$ and $n_0^* = 1.10$ for case B (line-point), and as computed from input $c(r)$ (dashed line). The corresponding results for case A are shown in the inset.

the pressure term. In case B, the complete model with both nonlinearities are included. The input $c(r)$ here corresponds to the full Lennard-Jones potential [14]. The results for $\mathcal{C}(q_m,t)$ at $T = 0.6$ and $n_0^* = 1.10$ corresponding to cases A and B are shown in Fig. 7. We extend the numerical solution to the longest possible time scale ($>10^3$ in LJ units) which is about four orders of magnitude beyond the microscopic time scales. The decay of the dynamic correlation is very different in the two cases and agrees with the previous theoretical results on the role of $1/\rho$ nonlinearity on the long time dynamics [1,8]. The static correlations in the two cases mentioned above are not very different, as is shown in Fig. 6 with the pair correlation function for the two cases mentioned above. The effects on the dynamic correlation on the other hand is rather drastic. Case A will give rise to the ideal transition model typically called the simple mode coupling model with a sharp ENE transition, while the full implication of all the density nonlinearities is obtained from case B.

The $1/\rho$ nonlinearity in the dynamics is a consequence of the form of the kinetic energy part F_K of driving free energy [see Eq. (6)]. Thus, case A above, in which the $1/\rho$ nonlinearity appearing in the equations for momentum density is replaced by $1/\rho_0$, would appear to follow from the purely Gaussian free energy or effective Hamiltonian with a kinetic energy term as

$$F_K = \int d\mathbf{x} g^2/(2\rho_0), \tag{19}$$

However, with a completely Gaussian free energy with F_K as above, the equations of motion for ρ and $\mathbf{g}$ are not those considered in case A. The NFH equations with a purely Gaussian free energy are obtained as

$$\frac{\partial \rho}{\partial t} + \rho_0^{-1} \nabla \cdot [\rho \mathbf{g}] = 0, \tag{20}$$

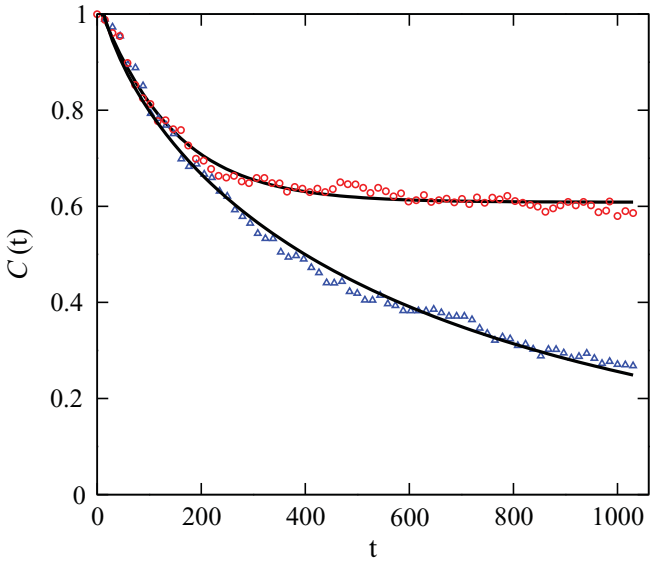

FIG. 7. (Color online) $\mathcal{C}(t)$ vs t/τ_0 at $T^* = 0.6$ and $n_0^* = 1.10$ for case A (circles) and case B (triangles). The solid lines are the best fit curves to the corresponding data.

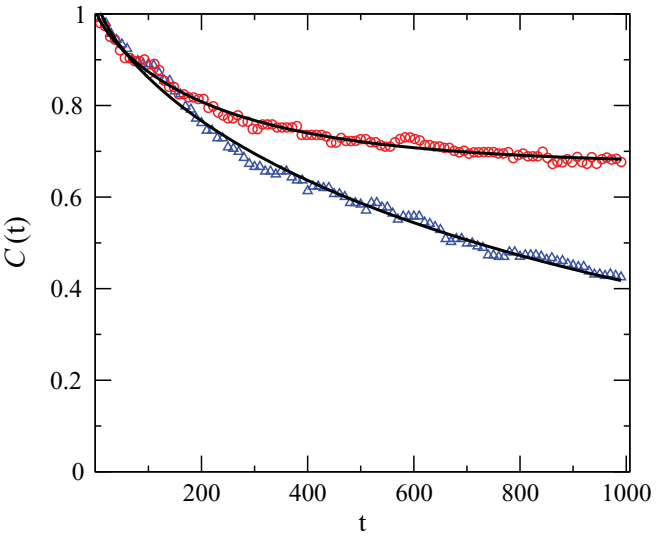

FIG. 8. (Color online) $\mathcal{C}(t)$ vs t/τ_0 at $T^* = 0.6$ and $n_0^* = 1.2$ for case A (circles) and case B (triangles). The solid lines are the best fit curves to the corresponding data.

and

$$\frac{\partial g_i}{\partial t} + \rho \nabla_i \frac{\delta F_U}{\delta \rho} + L_{ij} \frac{g_j}{\rho_0} = \theta_i. \tag{21}$$

Both Eqs. (20) and (21) are now nonlinear. The actual dynamics for the Gaussian free energy model is more involved and violates the continuity equation. In fact the nonlinearities in the density equation give rise to the same ergodicity restoring mechanism [15,16] as obtained in the models with $1/\rho$ nonlinearity. In case A, on the other hand, we have considered a completely linear dynamics apart from the nonlinearity in the pressure term. Even a purely Gaussian form of the potential or interaction part F_U of the effective Hamiltonian gives rise to the pressure nonlinearity. The kinetic part of the effective Hamiltonian does not influence this. The case A considered here is motivated to demonstrate the relative importance of the different nonlinearities appearing in the equation of the full model of case B. In Figs. 8 and 9 we show the same analysis being applied, respectively, at two more densities $n^* = 1.20$ and 0.9. At low density $\rho = 0.9$ the difference between the two cases is not much pronounced. On the other hand at higher density $n_0^* = 1.12$ the Nonergodicity parameter (NEP) value at which the density correlation freezes in case A is comparatively higher than at $n_0^* = 1.10$. These results are along expected lines with the analytical treatment of the problem [1,8].

With the application of coarse graining we are able to extend the study of the coupled dynamics of the slow modes up to times much longer than that of Ullo and Yip. We will focus here primarily on the relaxation behavior of the density correlation functions in the supercooled state. We have equilibrated the system for $\rho = 1.10$ and five different temperatures $T = 1.4$,1.2, 1.0, 0.9, and 0.8, all lying below the freezing point T_m(=1.86) [17] and in the vicinity of T_c. We have calculated the equilibrium correlation function $\mathcal{C}(t)$ from Eq. (16). The α relaxation time τ_α and the stretching exponent β at a given temperature are obtained by fitting a stretched exponential form [Kohlrausch-Williams-Watts (KWW)] to the equilibrium correlation functions $\mathcal{C}$(t). In order to obtain the equilibrium correlation functions we first made sure that the stage of time translational invariance was reached. For the temperature $T = 0.8$ (and above) as t_w becomes large the density correlation function becomes independent of the waiting time, and the plot of $C(t + t_w, t_w)$ vs t for different t_w overlaps. This behavior is displayed in Fig. 10. In the inset of Fig. 10, the $C(t + t_w, t_w)$ vs t_w plot for two fixed times $t = 200$ and 400 (in LJ units) shows clearly how the system equilibrates. The overlapping data for large t_w represents the equilibrium relaxation. The equilibrium curve fits well to a stretched exponential curve as shown by a solid line.

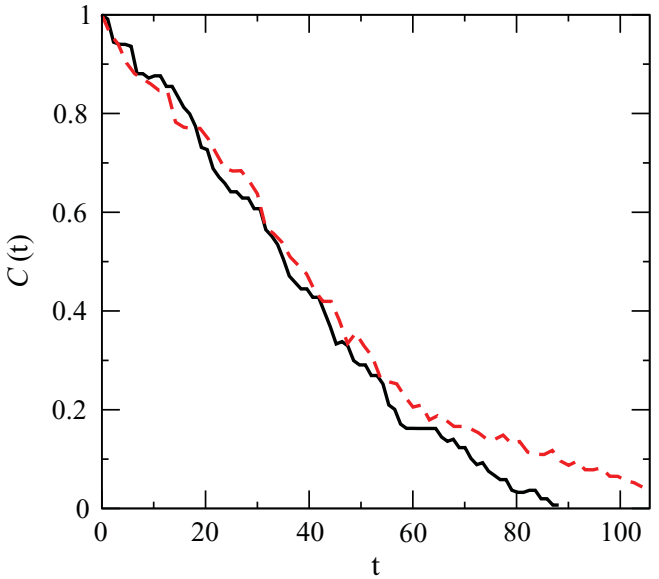

FIG. 9. (Color online) $\mathcal{C}(t)$ vs t/τ_0 at $T^* = 0.9$ and $n_0^* = 0.9$ for case A (dashed line) and case B (solid line).

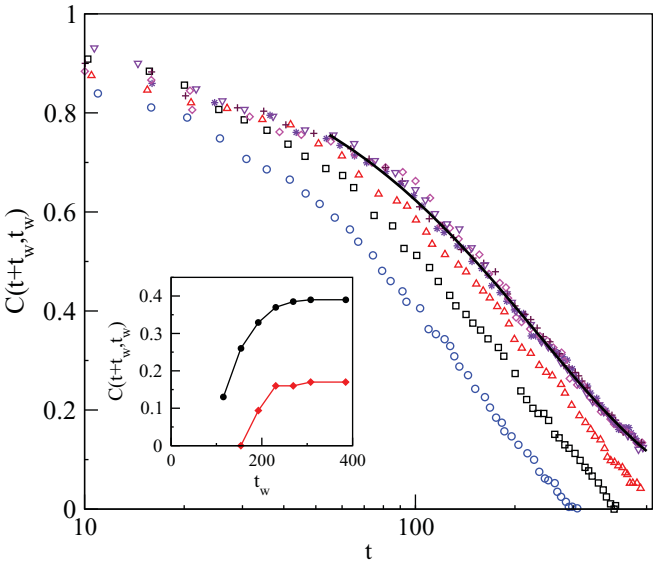

FIG. 10. (Color online) Variation of $C(t+t_w,t_w)$ as a function of t/τ_0 for $t_w/\tau_0 = 100$ (circles), 150 (squares), 200 (triangle up), 250 (stars), 300 (diamonds), 350 (plus), and 400 (triangle down) at $T^* = 0.8$ and $n_0^* = 1.10$. Solid line is the best fit curve of the overlapping data for large t_w having the KWW form. The variation of $C(t+t_w,t_w)$ as a function of t_w/τ_0 at time $t/\tau_0 = 200$ (circles) and 400 (squares) at $T^* = 0.8$ for density $n_0^* = 1.10$ is shown in the inset.

We have studied the equilibration of the system for even lower temperatures 0.7 and 0.6. For such low temperatures the relaxation time becomes large and we need to go to long waiting times (t_w) to reach a stage of time translational invariance. This is increasingly difficult for lower temperatures. Therefore we have adopted an extrapolation scheme to obtain the time translational invariant correlation function. For a fixed t we extrapolate the $C(q_m,t+t_w,t_w)$ at different t_w to obtain its value for large t_w. This is demonstrated in Fig. 11. For the lowest temperature $T = 0.6$ we observe two qualitatively

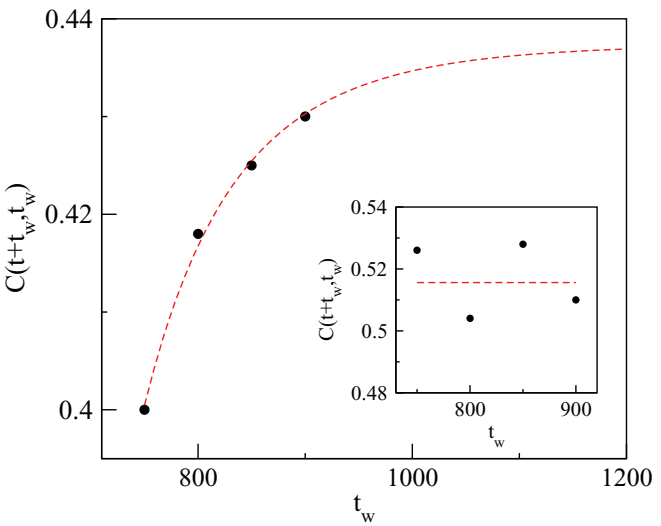

FIG. 11. (Color online) $C(t+t_w,t_w)$ vs t_w/τ_0 for temperature $T^* = 0.6$ and $n_0^* = 1.10$ at times $t/\tau_0 = 900$ (main graph) and 300 (inset) shown by circles. The dashed lines are the best fit curve.

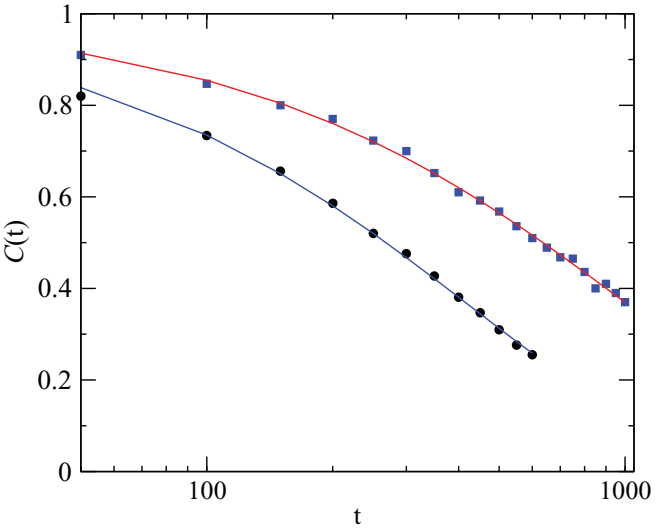

FIG. 12. (Color online) Equilibrated $\mathcal{C}(t)$ vs t/τ_0 for temperature $T^* = 0.7$ (circles) and 0.6 (squares) at $n_0^* = 1.10$. The solid lines are the best fit curves having the KWW form.

different kinds of t_w dependence. Up to a time $t < 650$ (in Lennard-Jones (LJ) units) we notice that the $C(q_m,t+t_w,t_w)$ vs t_w graph (at fixed t) randomly moves around a mean curve indicating overlapping curves in a $C(q_m,t+t_w,t_w)$ vs t plot (for different t_w). On the other hand for $t > 650$ (in LJ units), the t_w dependence of $C(q_m,t+t_w,t_w)$ asymptotically approaches a limit which is assumed to be its time translational invariant value.

This asymptotic value (for large t_w) represents the equilibrated value of $\mathcal{C}(t)$. The resulting curve $\mathcal{C}(t)$ vs t is shown in Fig. 12 for $T = 0.7$ and 0.6. The decay conforms to the stretched exponential form similar to what followed at higher temperatures, but with different exponents $\beta = 0.84$ and 0.69 for $T = 0.7$ and 0.6, respectively. Thus the stretching increases with the fall of temperature. The temperature

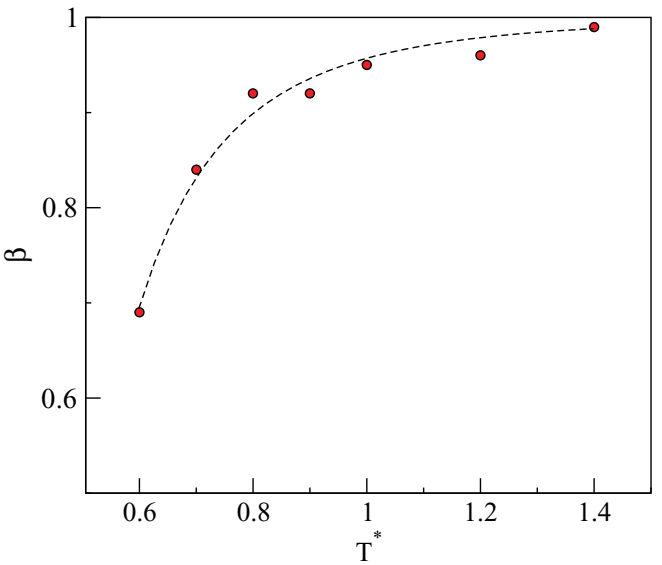

FIG. 13. (Color online) Variation of the stretching exponent β as a function of T^*. The dashed line is the best fit curve.

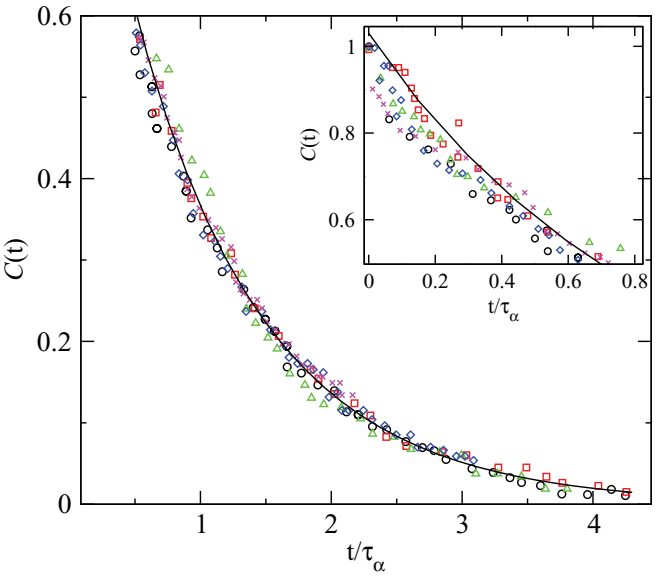

FIG. 14. (Color online) $\mathcal{C}(t)$ vs t/τ_α at $n_0^* = 1.10$ and temperatures $T^* = 1.4$ (circles), $T^* = 1.2$ (squares), $T^* = 1.0$ (triangles up), $T^* = 0.9$ (diamonds), $T^* = 0.8$ (stars). Solid line is the best fit to the overlapping function having the KWW form. The overlap of the short time data is not good, as shown in the inset.

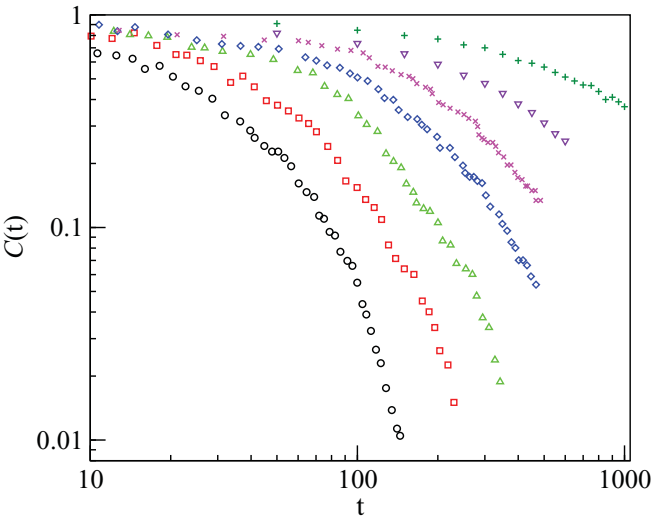

FIG. 15. (Color online) Variation of $\mathcal{C}(t)$ ($\log_{10}$ scale) vs t/τ_0 ($\log_{10}$ scale) at $n_0^* = 1.10$ and temperatures $T^* = 1.4$ (circles), 1.2 (squares), 1.0 (triangles up), 0.9 (diamonds), 0.8 (stars), 0.7 (triangles down), and 0.6 (pluses).

dependence of the stretching exponent β is shown in Fig. 13. Note that for the high-temperature regime the stretching exponent is weakly temperature dependent. Indeed for the high-temperature regime the data for different temperatures overlap as shown in Fig. 14, and the temperature-independent β which fits to this overlapping curve corresponds to the average value of β shown in Fig. 13. The equilibrium $\mathcal{C}(t)$ for different temperatures T decays with stretched exponential form $f\exp[-(t/\tau_\alpha(T))^\beta]$. Therefore the time temperature superposition works approximately in the high-temperature region, while in the deeply supercooled state it breaks down, with the stretching increasing as the temperature is lowered.

Since the relaxation is not over several time decades we also considered a fit in Fig. 15 to rule out the possibility of a power-law relaxation. We find the $\mathcal{C}(t)$ vs t curves (both in $\log_{10}$ scale) for different temperatures are nonlinear over the range at which we fitted them to the KWW form. In fact in the above fits of the correlation function obtained directly from the solution of the FNH equations, not much of the two-step relaxation process predicted in the one-loop mode coupling theory is displayed. It should be noted that the power-law behavior of the correlation function over the intermediate times requires that the system gets close enough to the ideal transition point of MCT. Therefore consideration of the equations with all the relevant nonlinearities implies a qualitatively different dynamics. We discuss this point further in the next section.

The α relaxation time τ_α is plotted with temperature in Fig. 16. In the temperature dependence we observe a power-law growth $(T - T_c)^{-a}$ with a $T_c^* = 0.34$ and exponent $a = 2.22$. We also attempt to fit the data with the Vogel-Fulcher form $\exp(\frac{B}{T-T_c})$ and find a $T_c = 0.27$. The quality of fitting in the two cases is shown in Fig. 16. The time translational invariance seen here for $T = 0.7, 0.6$ is valid over scales of the order of the corresponding relaxation time τ_α. The apparent divergence at T_c is removed at low temperatures. The value of the mode coupling transition temperature obtained from integral equations of the MCT [6] at one-loop order has the value $T_c = 1.05$ [18]. Thus the critical temperature falls with the nonperturbative calculation. This is in qualitative agreement with the trend seen in computer simulations [19].

V. DISCUSSION

We have shown that the direct numerical solutions of the NFH equations provide a reliable way of studying the

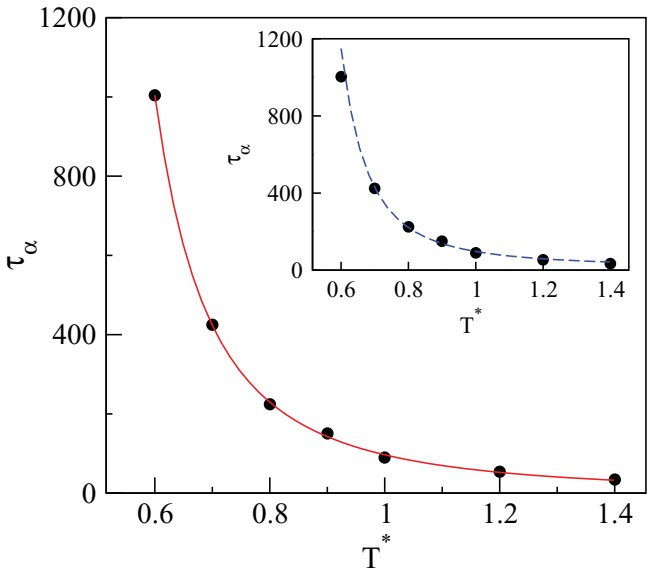

FIG. 16. (Color online) Relaxation time τ_α vs T^* (filled circles) fitted with a power-law (solid line) and Vogel-Fulcher (dashed line) form.

dynamics of fluctuations in a dense liquid in the vicinity of the avoided ergodic-nonergodic transition. The NFH equations studied here represent a coarse-grained description of the system in terms of a set of stochastic partial differential equations signifying basic conservation laws. This is different from a typical molecular dynamics simulation in which the actual dynamics of a small number of particles are tracked. The size of the box considered in the present work is about $\sim(4.3\sigma)^3$ and is not large compared to the typical MD simulation volume. However, it should be noted that we are solving the equations of motion for the densities $\rho(\mathbf{x},t)$ and $\mathbf{g}(\mathbf{x},t)$ over such length scales as compared to the case of solving actual particles being confined in boxes of this size. While the present method is not appreciably more efficient than molecular dynamics from a computational standpoint, it provides a way of investigating theoretical assumptions that are made in the analytical treatment of these equations. In particular our work clearly shows the role of the $1/\rho$ nonlinearity present in the dissipative term of Eq. (2) in restoring ergodicity [1] and is in agreement with previous analytic studies. The equations of fluctuating hydrodynamics studied here are obtained for a state which corresponds to a single fluid type minimum of the free energy and does not involve an activated process of hopping between states of different free energy minima. The present method can be easily extended to a larger set of hydrodynamic variables, which would permit a description of the dynamics in binary mixtures.

An important theoretical development in understanding the slow dynamics in the supercooled liquid coming from the liquid side is the mode coupling theory (MCT). The model equations for the MCT have been obtained [1,20] from the same NFH equations we studied here. In the MCT formulation the primary quantity of focus is the normalized density correlation $\phi(q,t)$ which acts as an order parameter in the theory. The Laplace transform of ϕ is written in terms of the renormalized viscosity $\Gamma^R(q,z)$ as

$$\phi(q,z) = \left[z - \frac{\Omega_q^2}{z + i\Gamma^R(q,z)} \right]^{-1},$$

where $\Omega_q^2 = q^2/[\beta m S(q)]$ is a microscopic frequency of the liquid state, and we use the initial value $\phi(q,t=0) = 1$. The crucial feedback mechanism for the MCT follows as a consequence of renormalization of the transport coefficient Γ^R due to the nonlinearities in the equations of motion of the slow modes. The nonlinearities in this case are in the equation for the momentum density $\mathbf{g}$. The equation for density ρ, i.e., the continuity equation, is linear in the fields. The strong enhancement of viscosity characteristic of the slow dynamics and the consequent ENE transition of simple MCT is driven by the nonlinear couplings of density fluctuations in the pressure term of the generalized Navier-Stokes equation. For the nonperturbative solution of the FNH equations considered here, if we include only the effects of this nonlinearity (case A above) then the correlation function shows a freezing over the time scales considered. On the other hand for the full model (case B) the density correlation function decays in agreement with the simulation results. We demonstrate here that the $1/\rho$ nonlinearity in the momentum equation plays a crucial role in the observed behavior. The numerical solution of the FNH equations also allows us to easily compute the correlation functions when the quenched liquid is evolving to equilibrium by choosing for the two point correlation function different values for the initial time.

The two-step relaxation is very closely related to the formation of a plateau in the relaxation over intermediate times. In the one-component system at the densities and over the time scale we could extend the solutions of the NFH equations, we do not observe a plateau. Nor does the simulation results of one-component systems show such a two-step decay. The corresponding time scales, namely, about 50 LJ units is not very small compared to that of the short time dynamics of such systems. We have extended the solutions by another order of magnitude in time but no plateau is seen. MD simulations of a simple two-component system (Kob-Andersen mixture) indeed shows a plateau over a couple of decades.

It should be noted that the NFH equations for such a system will be quite different from what we have solved here. Solutions of the more involved set of NFH equations for a binary system would settle such an issue and possibly demonstrate the role of single-particle dynamics in cage formation and occurrence of the plateau. Another related issue is that traditionally two-step relaxation is a prediction of the approximate MCT which follows from the NFH equations that we solve here numerically. And yet the two-step relaxation is absent here.

What is important to note is that it is only the simplified form of the MCT model (with a sharp ENE transition) for which this holds. Such a MCT model ignores all other processes other than the density nonlinearity driving the system to a ergodic-nonergodic transition. It is *simply assumed* that the ergodicity restoring processes are absent. From our observation of the solutions of the NFH we do not see that such an assumption holds in the one-component system that we consider here. Indeed, as already noted and observed by others [22,23] working with microscopic models, if the magnitude of the ergodicity restoring mechanism or the so-called hopping kernel does not decrease upon supercooling, much of the dynamical behavior predicted by the original MCT gets masked, and the meaning of the special temperature T_c becomes questionable.

In closing this discussion on the NFH equations for a liquid, it is useful to consider a similar model for slow dynamics of supercooled liquids that has often been used in recent literature. This is the so-called dynamic density functional theory (DDFT) model involving a single stochastic equation for the coarse-grained density $\rho(\mathbf{x},t)$ with multiplicative noise. This equation [21] isreached starting from the NFH equations used in the present paper and integrating out the momentum field $\mathbf{g}(\mathbf{x},t)$ within the so-called adiabatic approximation. As a consequence of this, the $1/\rho$ nonlinearity is eliminated from the problem and the simple noise in the $\{\rho,\mathbf{g}\}$ formulation gets changed into multiplicative noise for the single ρ equation. At the one-loop order of renormalization, this model (with the FNH equation for the density variable only) also predicts a sharp ENE transition. This is similar to the dynamic transition in the mode coupling model (considered in the present work) obtained from the $\{\rho,\mathbf{g}\}$ formulation with simple driving noise. However, the complete description of the dynamics following

from this DDFT model equation is still unclear. Here one does not face the $1/\rho$ nonlinearity but the driving noise is multiplicative noise [24]. The mechanism for the sharp ENE transition being finally smoothed out would require extending the analysis further. This will require doing a proper analysis of the perturbative field theory corresponding to the nonlinear equation for $\rho(\mathbf{x},t)$ with multiplicative noise and possibly inclusion of higher loop corrections in the perturbation theory. Solving these equations in a manner similar to what we have done in the FNH case with additive noise will be a useful step in understanding this problem. These two models may belong to the same dynamic universality class, though applying the critical phenomena terminology will not be totally appropriate in this context.

ACKNOWLEDGMENTS

CEFIPRA is acknowledged for financial support under the Indo-French research project 2604-2. B.S.G. acknowledges CSIR, India, for financial support.

[1] S. P. Das and G. F. Mazenko, Phys. Rev. A **34**, 2265 (1986).
[2] A. Andreanov, G. Biroli, and A. Lefevre, J. Stat. Mech, (2006) PO7008.
[3] T. N. Nishino and H. Hayakawa, e-print arXiv:0803.1797v2.
[4] B. Kim and K. Kawasaki, J. Stat. Mech, (2008) P02004.
[5] U. Bengtzelius, W. Götze, and A. Sjölander, J. Phys. C **17**, 5915 (1984).
[6] S. P. Das, Rev. Mod. Phys. Rev. **76**, 785 (2004).
[7] D. R. Reichman and P. Charbonneau, J. Stat. Mech., (2005) P05013.
[8] S. P. Das and G. F. Mazenko, Phys. Rev. E **79**, 021504 (2009).
[9] J-P. Hansen and I. R. McDonald, *Theory of Simple Liquids*, 3rd ed. (Academic, New York, 2006).
[10] T. V. Ramakrishnan and M. Yussouff, Phys. Rev. B **19**, 2775 (1979).
[11] L. M. Lust, O. T. Valls, and C. Dasgupta, Phys. Rev. E **48**, 1787 (1993); O. T. Valls and G. F. Mazenko, Phys. Rev. A **46**, 7756 (1992).
[12] J. J. Ullo and S. Yip, Phys. Rev. Lett. **54**, 1509 (1985).
[13] Shankar P. Das, Phys. Rev. A **42**, 6116 (1990).
[14] Contrast this to the input $c(r)$ for Fig. 2. Hence the slight difference between the results of case A in Fig. 3 and that of the solid line of Fig. 2.
[15] R. Schmitz, J. W. Dufty, and P. De, Phys. Rev. Lett. **71**, 2066 (1993).
[16] S. P. Das, Phys. Rev. E **54**, 1715 (1996).
[17] S. P. Singh and S. P. Das, J. Phys. Condens. Matter **19**, 246107 (2007).
[18] S. P. Singh and S. P. Das, Phys. Rev. E **79**, 031504 (2009).
[19] W. Kob and H. C. Andersen, Phys. Rev. E **51**, 4626 (1995).
[20] T. R. Kirkpatrick and J. C. Nieuwoudt, Phys. Rev. A **33**, 2651 (1986).
[21] K. Kawasaki and S. Miyazima, J. Phys. B Condens. Matter **103**, 423 (1997).
[22] C. Z. Liu and I. Oppenheim, Physica A **235**, 369 (1997).
[23] J. Yeo, Phys. Rev. E **80**, 051501 (2009).
[24] The NFH equations we are dealing with here or those which Kawasaki obtained by integrating out the momentum field **g** are for the (coarse-grained) physical density field $\rho(x,t)$. They satisfy stochastic partial differential equations which are phenomenological and are irreversible for both Newtonian dynamics and Brownian dynamics. This is different from the single stochastic equation for the density which was obtained by D. S. Dean, J. Phys. A: Math. Gen. **29**, L613 (1996). for a system of particles following microscopic Brownian dynamics. Dean's equations are an exact stochastic representation of the evolution of the *formally defined* density field $\hat{\rho}(x,t)$ (expressed in terms of the sum of Dirac δ functions) for Brownian interacting particles. This exact equation is a microscopic balance equation reflecting the microscopic conservation law. Indeed in a similar way, for the microscopic (reversible) Newtonian dynamics the corresponding *exact* balance equations are the reversible Euler equations. In the Brownian case the balance equation is dissipative since the corresponding microscopic dynamics is also irreversible. This balance equation of Dean apart from the similar form as Kawasaki's coarse-grained equations is driven by different force terms with different free energy functionals. The physical correlation functions which would result according to the Kawasaki equation of DDFT can not be alternatively obtained *in an exact manner* by doing molecular dynamics simulation of Brownian particles.